Controlled solvent-exchange deposition of phospholipid membranes onto solid surfaces

Andreas O. Hohner, Maria Pamela C. David, and Joachim O. Rädler[a)]

Centre for Nanoscience and Fakultät für Physik, Ludwig-Maximilians-Universität, Geschwister-Scholl-Platz 1, München D-80539, Germany

Controlled deposition of lipid bilayers plays a key role in creating supported membranes for biosensing devices and biophysical cell studies. The authors adopt a solvent-exchange method in order to deposit a phospholipid bilayer on solid substrates. The basic concept of deposition is to dissolve phospholipids in isopropanol-water mixtures and to increase water content gradually. Shortly before the onset of the micelle-to-vesicle transition, a lipid bilayer nucleates at the solid surface. They investigate the bulk phase behavior and surface coverage using small angle x-ray scattering and attenuated total reflection-Fourier transform infrared spectroscopy. They find a sequence of transitions from inverted-monomeric-micellar and vesicle phases correlating with an increasing amount of lipid on the adsorption layer. Supported lipid bilayers, prepared using this approach, are homogeneous and fluid. © *2010 American Vacuum Society.*
[DOI: 10.1116/1.3319326]

I. INTRODUCTION

Many of the structural and dynamical properties of lipid bilayers, which characterize the unique properties of biological membranes, can be preserved when deposited on solid surfaces. As advocated in a seminal article by Sackmann,[1] the scientific and practical applications of supported membranes are versatile, and include applications such as biophysical model systems, biosensors or phantom cells. In general, molecules and their molecular interactions are more easily detected or imaged when anchored to surfaces. Supported membranes can be prepared as lipid monolayer or bilayers. They can be chemically grafted to the solid or adsorbed due to unspecific surface interactions. These have the potential to be used in various ways in combination with structured surfaces.[2–8] For instance, it is possible to confine fluid corals to chemically defined fields.[6] This allows the creation of integrated devices, such as lipid arrays or parallel assays in lipid-based chips for analytical and diagnostic applications.[2,4,5] Moreover, supported membranes can be combined with electrodes for monitoring membrane impedance of pores,[7,9] or with semiconductor technology for the application of lateral fields for membrane based electrophoresis.[2,10,11] Since supported membranes remain fluid, adsorbed macromolecules can easily be rearranged, permitting DNA molecules to be prepared in a stretched state.[12] Setups required for observing and manipulating the spatial organization of cell-model membrane interactions benefit from supported membranes in that the interacting components are well presented, such as those involved in the specific immunological recognition processes of T-cells.[13] An important role of lipids is also expected in future nano-biosystems. Here, supported membranes can be designed with nanoscale precision as nanofluidic lanes for transporting and monitoring single molecules.[8,14]

There are various methods by which supported lipid bilayers (SLBs) can be deposited on surfaces. SLBs are commonly prepared by vesicle fusion, a method developed in the McConnell laboratory,[15,16] where sonicated vesicles in contact with an appropriately cleaned glass surface rupture and spread out to form a continuous bilayer.[17] The difference in surface free energy between a bare and lipid bilayer-coated glass surfaces under water is the driving force that drags the bilayer from an area of excess lipid to uncovered areas.[18,19] Other methods to prepare supported membranes include the Langmuir–Blodgett deposition,[15] spin coating,[20] evaporation induced self-assembly,[21] and more recently, dip-pen technology.[8] Each of these methods has inherent advantages with respect to the applications in which they will be used. For instance, the Langmuir–Blodgett deposition allows the deposition of asymmetric bilayers,[22] dip-pen technology facilitates the fabrication of biomolecular arrays,[8] spin coating enables the quick generation of highly oriented, homogeneous bilayer stacks with defined thickness,[20] and evaporation induced self-assembly permits the creation of patterned nanocomposites of dissimilar materials.[21] In some applications, exposure of the sample to air should be avoided, and solution-based deposition of supported bilayers is preferred;[22] such procedures would also be suitable for a wider class of surfaces, including hydrophobic surfaces[23] or, in principle, also solid particles such as silica or glass beads.[24,25] Tiberg *et al.*,[26] for example, reported a simple method of this kind for preparing model lipid bilayers by coadsorption with a nonionic surfactant.

In this article, we present a solvent exchange method to prepare supported membranes. In this process, the quantity of the organic solvent, in which the lipids are dissolved, is continuously varied by addition of water. The approach is inspired by the reverse-phase evaporation method, where liposomes are produced through the slow removal of organic solvent from a water-solvent mixture.[27] Specifically, we in-

---
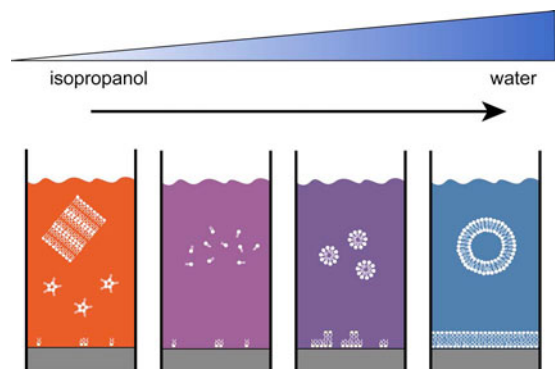[a)]Electronic mail: joachim.raedler@physik.uni-muenchen.de

FIG. 1. (Color online) Principle of solvent exchange-induced physisorption. Lipids dissolved in pure alcohol are not adsorbed onto a SiO$_2$ substrate. As water content increases, micelles begin to form, which can also adhere to the substrate. In pure water, lipid bilayers exist both on the substrate, as well as in solution (as liposomes).

vestigate the lyotropic phases of lipids in isopropanol-water mixtures and the degree of lipid adsorption to solid surfaces as a function of increasing water content (i.e., solvent exchange), as schematically depicted in Fig. 1. Isopropanol was chosen from the commonly used solvents because of its complete miscibility with water. The lipids 1,2-dimyristoyl-*sn*-glycero-3-phosphocholin (DMPC) and 1,2-dimyristoyl-*sn*-glycero-3-trimethylammoniumpropan (DMTAP) were chosen to investigate the effect of lipid charges on structure formation on negatively charged surfaces. We present data obtained using small-angle x-ray scattering (SAXS) and attenuated total reflection (ATR) infrared spectroscopy to determine the bulk phase behavior and the degree of surface adsorption. A micelle-to-bilayer transition was found to occur at water contents between 80% and 90%. It is shown that a continuous fluid lipid bilayer deposits at glass surfaces when the water content of a lipid/alcohol/water mixture is gradually increased across this transition point.

II. MATERIALS AND METHODS

A. Reagents

DMPC and a cationic lipid, DMTAP, as well as its equivalents with deuterated fatty acid chains (d54-DMPC and d54-DMTAP), were purchased from Avanti Polar Lipids (Alabaster, USA). A lipid with a longer chain, l-stearoyl-2-oleoyl-*sn*-glycero-3-phosphocholine (SOPC, 18:0/18:1—phosphatidyl choline), was also obtained from Avanti Polar Lipids. All lipids were delivered dissolved in chloroform. Isopropanol was obtained from Fluka (Buchs, Switzerland). All compounds were used without further purification.

B. Lipid preparation

Lipid samples were prepared by evaporation of the chloroform under a nitrogen flow and subsequent storage of the dried lipid in vacuum overnight. Degassed water and isopropanol were mixed by their volume properties and added to the lipid. For Fourier transform infrared (FTIR) measurements, the lipids were dissolved in a mixture with the final water:isopropanol volume ratio. Samples for SAXS measurements were prepared similarly in cylindrical tubes with an outer diameter of 1.0 mm and wall thickness of 0.01 mm (Hilgenberg, Malsfeld, Germany).

For the continuous bleaching experiments, 2 mg lipids were tagged with 0.25 mol % Oregon green (Invitrogen) and dried overnight, as previously described.[24] Lipids were then initially dissolved in 1 ml of 50:50 (volume ratio) water:isopropanol solution and introduced into 100 μl Ibidi bottomless chambers (Ibidi, Munich) fitted with a silicon oxide surface (Roth, Germany). These surfaces were prepared by sonication in 2% Hellmanex for 15 min, followed by washing with sonication in distilled, de-ionized water (Mill-Q, Millipore Co., USA). All surfaces were dried under a nitrogen stream prior to use. Samples were slowly titrated with water, with 10 min intervals prior to the addition of water that changes the content 5% at a time, until a 90% content is reached. After the last titration, this system was allowed to equilibrate for 30 min prior to washing and measurement. Samples were washed at least five times prior to measurement to ensure the removal of remaining vesicles.

C. FTIR

ATR-FTIR experiments were performed with a Nicolet 60SXR FTIR spectrometer with a self-developed horizontal ATR flow cell. The cell consists of a polycarbonate window to avoid the formation of air bubbles and an aluminum crystal holder for a water-based temperature control.

To imitate a glasslike substrate a silicon crystal with a native SiO$_2$ surface was used as the ATR crystal. The silicon crystal's surface was purified by storing it in a 2% sodium dodecyl sulfate solution for one day and cleaning it in a mixture of 70% nitric acid, 10% hydrogen peroxide, and 20% water for 1 h. The crystal was rinsed under water and dried for one day. Infrared spectra $I_B(\nu)$ of the dry cell, $I_R(\nu)$ of the water/isopropanol filled cell, and $I_S(\nu)$ of the cell filled with lipid and solvent were measured. The corrected spectra were calculated by

$$I = \frac{I_s}{I_B} - \kappa \frac{I_R}{I_B}.$$

The coefficient κ was adjusted to minimize the water bands in the spectra.[28] For each lipid mixture, a part of the sample and the reference measurements are used in order to prevent the retention of any background after the correction. Lipids used had a concentration of 1 mg/ml. A 15 min equilibration period is allotted after samples are placed in the measurement chamber; this also allows the water vapor and CO$_2$ in the chamber to be reduced.[29] To determine the absorption intensities, the spectra were matched against a sum of six Gaussian curves, with their position and width determined from reference measurements involving higher lipid concentrations. For the analysis, a prefactor was varied and data were fitted with a Gaussian-type baseline correction.

D. SAXS experiments

SAXS experiments were carried out at the high brilliance beamline ID2 at the ESRF (Grenoble, France). X-ray scattering intensity at 0.15 nm was measured by a multiwire proportional gas-filled detector and radial integrated. The investigated q range for SAXS was 0.2–5 nm^{-1}. The sample environment allowed temperature control within 0.1 °C through a Peltier water bath setup. The rotational symmetric scattering data were integrated radially and fitted with a model of three definite electron densities for solvent, acyl chains, and headgroup. Scattering curves were fitted in the wave vector range between 0.8 and 5 nm^{-1} without background correction. The headgroup of the lipids was assumed to consist of an electron density $>_H = 0.45$ $e^-/$Å^3 and acyl chains of $>_c = 0.17$ $e^-/$Å^3.[30,31] The electron densities of isopropanol-water mixtures range from $\rho_0 = 0.157$ $e^-/$Å^3 (0% water) to 0.266 $e^-/$Å^3 (100% water).

E. Determination of the lyotropic phases

The multilamellar phases were characterized by the position of the Bragg peaks $d = 2\pi/q$ with no further analysis of the structure and form factor.[32–34] Isotropic phases were analyzed by fitting the intensity $I(q) = F(q)^2$ with the theoretical form factors $F(q)$, corresponding to spherical micelles, elliptical micelles, rodlike micelles, vesicles, and a planar lipid bilayer. The geometrical parameters were optimized to fit the data. In each case, the model with the best chi-square value was chosen. The form factor of vesicles was derived from the form factor of a sphere

$$F_s(\rho,\rho_0,R,q) = \left(\frac{4}{3}\pi R^3\right)(\rho - \rho_0)$$
$$\times \left[\frac{3 \sin(Rq) - Rq \cos(Rq)}{(Rq)^3}\right].$$

The form factor of a spherical micelle is than given by

$$F_v(\rho_H,\rho_0,R,D,q) = F_s(\rho_H,\rho_0,R,q) - F_s(\rho_H,\rho_C,R-D,q),$$

where ρ_H, ρ_c, and ρ_0 denote the electron densities of the lipid head group, the alcyl chains, and the solvent, respectively, and where R is the radius of the micelles. The form factor of a vesicle consists of several shells,

$$F_v(\rho_s,\rho_0,R,D_1,D_2,q) = F_s(\rho_H,\rho_0,R,q) - F_s(\rho_H,\rho_c,R$$
$$- D_1,q) + F_s(\rho_H,\rho_c,R+D_1$$
$$- D_2,q) - F_s(\rho_H,\rho_c,R+D-D_2,q).$$

D_1 and D_2 are the thickness of the headgroup and the membrane thickness, respectively. Elliptical micelles were fitted with the anisotropic form factor

$$F^2(\rho_c,\rho_s,\rho_0,R_c,R_s) = \int_0^{\pi/2} [V_c(\rho_c - \rho_s)f(q,R_c) + (V_s + V_c)$$
$$\times (\rho_s - \rho_0)f(q,R_s)]^2 \sin \Theta d\Theta,$$

$$f(q,R) = 3\frac{\sin X - X \cos X}{X^3},$$

$$X = qR\sqrt{\sin^2 \Theta + \varepsilon^2 \cos^2 \Theta},$$

$$V = 4/3\pi\varepsilon R^3,$$

where ε denotes the anisotropy factor.

F. Continuous bleaching

The continuous bleaching method[24,35,36] was used to characterize the dynamics of the generated membranes. According to the theory of the method, the spatial intensity of a fluorescently labeled membrane is described by simultaneous photobleaching and replenishment of fluorescent molecules as they diffuse in two dimensions. Briefly, we continuously illuminate a defined region [with an approximate diameter of 180 μm, viewed at 63$\times$ magnification, Figs. 7(a) and 7(e)] of the SLB, resulting in the bleaching of the Oregon green dye, whose fluorescence intensity at the center of the illuminated area, $I_{d/2}$, decays exponentially as a function of exposure time according to the equation

$$I_{d/2}(t) = I_{t_0}e^{-B_0 t} = I_{t_0}e^{-\tau},$$

where I_{t0} is the initial fluorescence intensity at the center of the illuminated area, B_0 is the bleaching rate, and $\tau = B_0 t$ is the dimensionless time. Values for $I_{d/2}$ and B_0 were obtained as previously described.[31] When the fluorescence intensity at the center of the illuminated region approaches background fluorescence, the fluorescence intensity line profile [Figs. 7(c) and 7(g)] is fitted as a function of distance according to the equation

$$I_x = I_{x_0} \cosh\left[\sqrt{\frac{B_0}{D}}\left(x - \frac{d}{2}\right)\right] + A_2',$$

where I_{x0} is the fluorescence intensity at the edge of the rim, D is the diffusion constant, and A_2' is a constant used in fitting. Diffusion constants are estimated from these fits [Figs. 7(c) and 7(f)]. SLBs formed by controlled deposition were compared to SLBs formed by vesicle fusion, as described by Zantl.[37]

III. RESULTS AND DISCUSSION

A. Determination of volume phases by SAXS

We used SAXS in order to determine the lyotropic mesophases of lipids through the whole spectra of water:isopropanol concentration ratios, as well as through different temperatures. Figure 2 shows the scattering intensities of the lipid, DMTAP, dissolved in water:isopropanol mixtures through increasing water concentration. In pure isopropanol, we find a sharp Bragg reflection at 1.42 nm^{-1}, corresponding to a structural periodicity of 4.4 nm. The periodicity increases to 4.7 nm when the water content is increased to 15%. These values lie within the bounds of typical values for a lamellar phase. However, the detailed structure of the
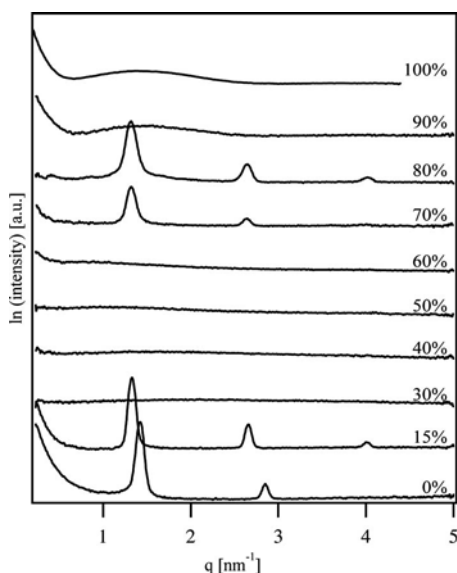
FIG. 2. DMTP scattering data for isopropanol-water solutions at 25 °C containing different amounts of water. The system goes from a lamellar phase in pure isopropanol and moves toward monomers and micelles, and eventually to a liposomal phase as the water content of the solvent increases. Data are plotted on a logarithmic scale.

lamellar phase in isopropanol might be distinct from the well-known lamellar phase of lipids dispersed in water.[38]

For 30% and 40% water contents (Fig. 2), no notable signals can be observed. These suggest a homogeneous scattering medium. A light bending that occurs maximally at 1.8 nm^{-1} corresponds to a distance of 3.5 nm, which is the characteristic correlation length for molecules at a concentration of 25 mg/ml. These features are both indicative of the

existence of lipid monomers. At 50% water content, a slightly increased intensity can be observed at 1 nm^{-1}, which may be indicative of a small fraction of micelles in solution. At 60%, the scattering profile exhibits a form factor which can be attributed to spherical micelles. The data were fitted to the form factor of a micelle in the range between 0.6 and 5 nm^{-1}, as described in the experimental section. Micellelike structures are known to occur in binary isopropanol-water mixtures, without lipid, at 60% water content.[38,39] It is likely that in the ternary system, phospholipids will incorporate into these spherical aggregates. Our data are consistent with a polydisperse, Gaussian distributed system of spherical micelles with a radius of 2.5 nm ± 1 nm and a headgroup size of 0.2 nm. These data were derived from SAXS data assuming a core-shell structure as described in the experimental section.

At 70% and 80% water contents, Bragg reflections associated with a multilamellar phase were detected again, with a periodicity of 4.8 nm. At 90%, we find a form factor corresponding to dispersed unilamellar vesicles [Figs. 2 and 3(b), and as described in the experimental section]. In this case, the fitting analysis yields a range of possible fit parameters dependent on the selected size distributions, as well as on the electron density. However, values for the thickness of the lipid bilayer varied around a value of 4.5 nm. The data are consistent with an average vesicle radius ranging from 20 to 100 nm. The inaccuracy of the fit with respect to the vesicle radius is possibly indicative of high polydispersity.

The abundance of DMTAP-isopropanol-water phases becomes even greater as the temperature is varied. As shown in Fig. 4(a), a region of inverted spherical micelles appears when the temperature is changed. Here, the radius of a mi-
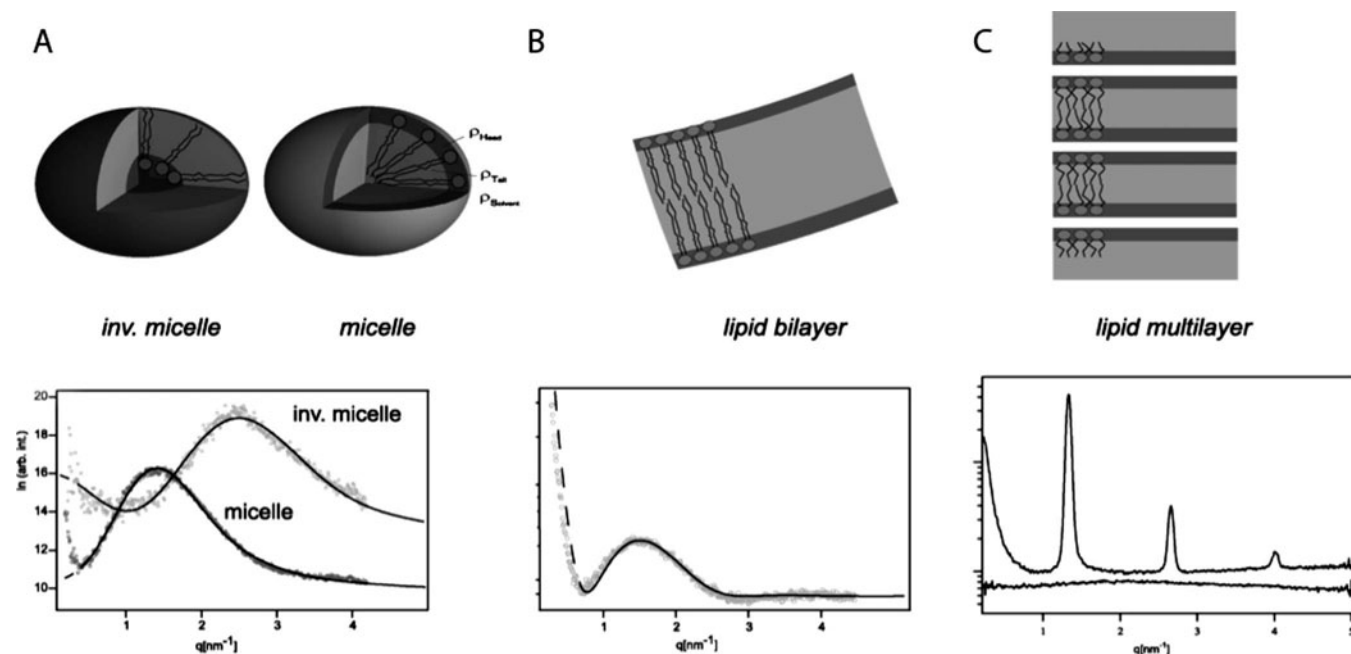

FIG. 3. Scattering data and corresponding form factor fits for various lipid structures in a DMTAP solution, such as micelles and inverse micelles at 60% water content (a), lipid bilayers at 90% water content (b), and multilamellar phases at 15% water content (c). The monomeric phase, which has essentially no signal, is contrasted with the multilamellar phase (c).
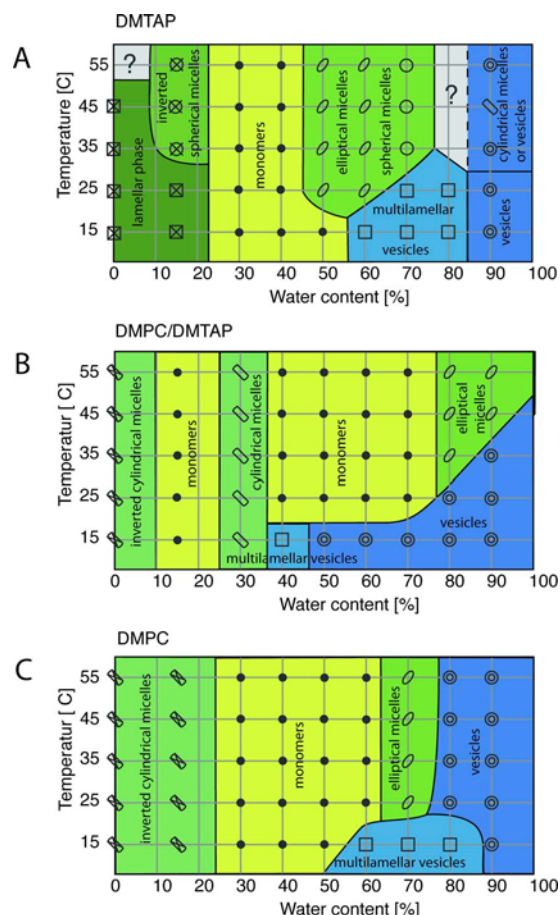
FIG. 4. (Color online) Phase diagrams for DMTAP (a), DMPC/DMTAP (b), and DMPC (c) with reference to varying isopropanol-water content and temperature. Lipids used in these measurements had a constant concentration of 25 mg/ml.
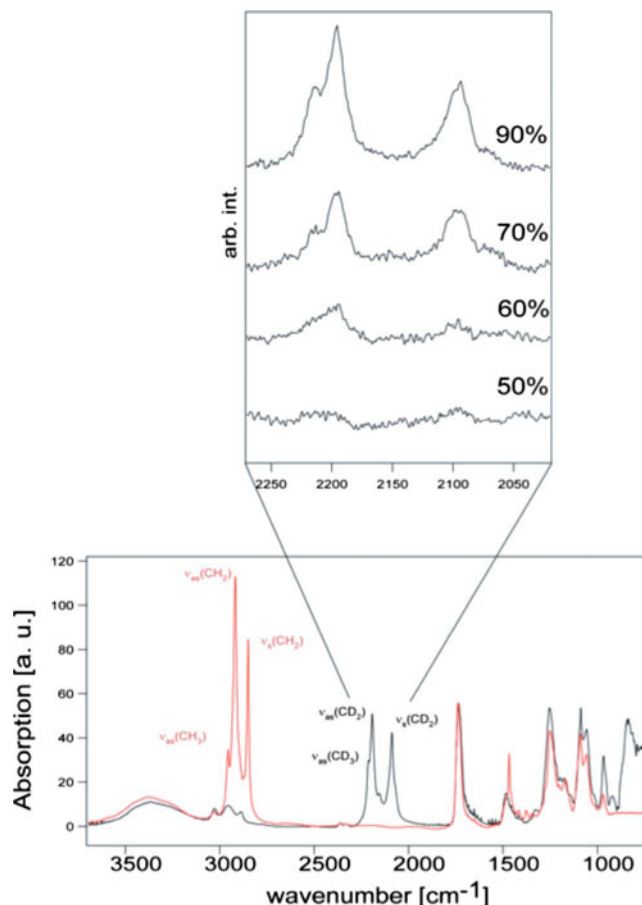

FIG. 5. (Color online) Infrared spectra showing the C–H and C–D stretching vibrations of DMPC (red line) and d54-DMTAP (black line, inset). The C–D stretching vibrations in the ATR mode are shown in the expansion as a function of increasing water content.

celle is around 2 nm, with a size distribution width of 0.1 nm. In Secs. III B–III D, we discuss phase behavior as a function of water content, temperature and lipid composition.

B. Bulk phase diagrams

Complete phase diagrams of DMTAP, DMTAP/DMPC, and DMPC as a function of water-isopropanol content and temperature are shown in Fig. 4. All phase divisions have degrees of uncertainty of 5 °C and 5% water content since phase transitions were not measured along the full division; measurements were instead made in representative points in the phase diagram. Areas with a question mark could not be described using commonly used form factors. The phase behavior reveals a general phase order: With increasing water content, inverse micelles, monomer, micelles, and finally, vesicles can be found. This behavior is clearly represented by the phase diagram of DMPC. In all three phase diagrams, regions where the lamellar phase occurs can be seen at lower temperatures.

Upon the addition of DMTAP to DMPC, the phase behavior becomes more complex. The phase diagram for a 1:1 DMPC-DMTAP mixture [Fig. 4(b)] differs from the DMTAP diagram in terms of the absence of the lamellar phase at low

water content. Furthermore, higher water content is required for the micelle phase to occur. In pure isopropanol, the lipid mixture exists as inverted cylindrical micelles. On reaching a water content of 15%, a transition to monomer phase is achieved, which could in turn undergo a transition to cylindrical micelles once the water content is increased to 30%. It is remarkable that vesicles at high water content but elevated temperatures are no longer stable. In the same regime, DMTAP exhibits phases that were not unambiguously determinable. Since we are interested how one can enter vesicle phases, it is remarkable that DMTAP/DMPC exhibits a temperature-induced transition from monomer to vesicles at water content of ≥50%.

C. Lipid surface coverage measured by ATR-FTIR

In this section, we discuss the adsorption of lipids from the bulk phase described above to silicon oxide as a function of water content. To distinguish the lipid from isopropanol, we used phospholipids with deuterated alcyl chains, which allow the determination of the degree of adsorption through specific infrared adsorption bands from ATR-FTIR. Figure 5 shows a bulk infrared spectrum of DMPC and deuterated d54-DMPC indicating the position of the C–H and C–D

stretching bands. The position of the C–H bands overlaps with the adsorption bands of isopropanol and cannot be used. The C–D stretching bands of the lipid, however, can be detected in the ATR mode, despite a broad background signal arising from water and isopropanol in bulk solution. Consequently, reference measurements were made for each sample, and a corrected spectrum is obtained, as described in the experimental section. The expansion in Fig. 5 shows typical results from a series of ATR-FTIR measurements.

Surface occupancy is proportional to the intensity of the alkyl bands. To determine this intensity, the spectra were matched against a sum of six Gaussian curves, which match the shape of the adsorption band fingerprint. In the fit, the amplitude of this set of Gaussians was taken as a measure of the degree of lipid coverage. The position and width of the set of Gaussians were independently determined from reference measurements, where higher lipid concentrations were used. Figure 6 shows the isothermal adsorption of DMTAP. Results are normalized to 1.0 at 100% water content, corresponding to the surface coverage obtained from vesicle fusion, i.e., a single lipid bilayer. An arc-tan fit, which serves as a visual guide, is overlaid across the adsorption isotherm as a function of water content. For DMTAP, the point at which half-surface coverage can be observed appears to be at 67% water content.

In the case of DMPC, a significantly shallower isotherm is observed, which does not have a defined transition point. Half-maximum coverage is found at approximately 40% water content; finite adsorption is observable even in pure isopropanol (0% water). In the case of the equimolar lipid mixtures of DMPC-DMTAP, the transition occurs between 63% water content. In comparison with pure DMTAP and pure DMPC, this approximates a behavior that is between the two. Figure 6(c) also indicates the percentages of DMPC and DMTAP separately. These data can be obtained if only one of the lipid components is deuterated. More interestingly, there is always a larger amount of DMPC than DMTAP adsorbed to the oxidized silicon surface. Infrared spectroscopy results indicate that the addition of water causes lipids dissolved in isopropanol to adhere to the hydrophilic silicon oxide surface. These ATR-FTIR results, however, do not reveal details of the quality of the lipid coating, specifically its homogeneity and its lateral diffusion.

D. Adsorption behavior of a thermotropic system

SAXS results imply that lipid adsorption can be induced not only through changes in solvent composition but through temperature changes as well. This strong temperature-dependent behavior is manifested through an increased degree of coverage for lower temperatures. If DMTAP in a 90% water:isopropanol solution is heated to 45 °C, all the lipids desorb. Upon cooling, a lipid bilayer is readsorbed, with increased coverage compared to before heating. In order to confirm if this effect on coverage is characteristic of the system or if it is an artifact of the prolonged equilibration period, DMTAP samples at different water contents are warmed from 10 to 50 °C and then cooled to 10 °C again.
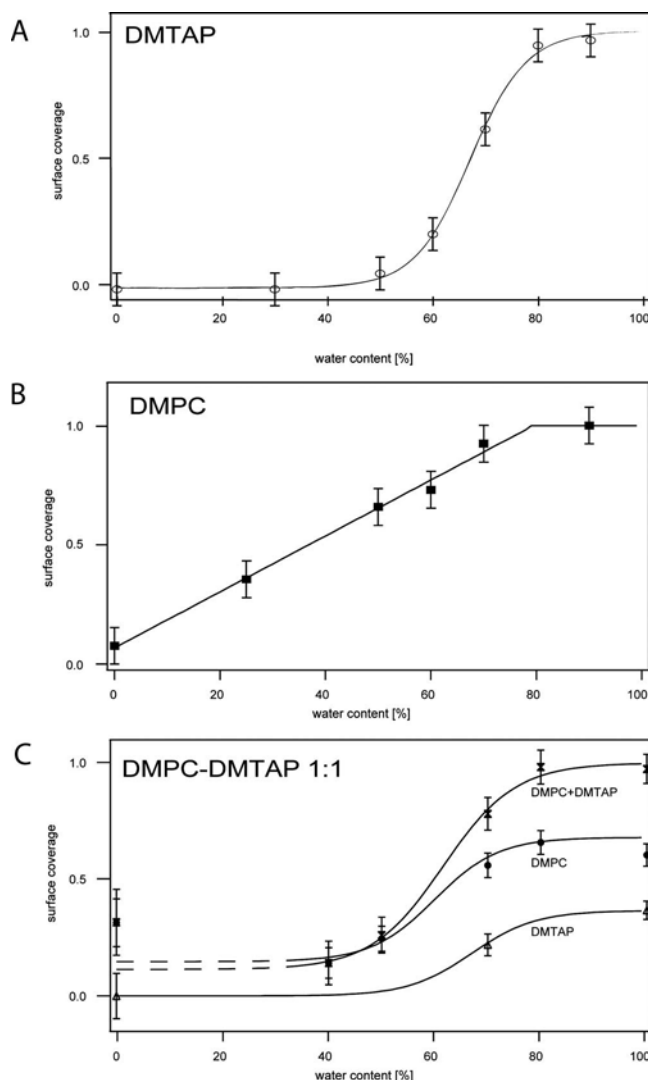

FIG. 6. Isothermal adsorption curves for d54-DMTAP (a), d54-DMPC (b), and d54-DMPC/d54-DMTAP (c) at 28 °C under varying water content. C–D stretching vibration intensities were normalized, and correspond to the lipid concentration on the silicon surface. The error bars are taken from the fits of the spectra; for multiple measurements, errors were calculated according to the rules of error propagation.

Surface coverage was checked at intervals of 10 °C during the process of heating, as well as after cooling. Results confirmed the initial observation on the temperature-dependence of coverage (data not shown). In terms of the phase changes, our hypothesis is that increasing the temperature at 90% water content results in transitions from the vesicle/bilayer phase to a mixed micelle and vesicle phase [Fig. 4(a)], and it is possible that the micelles generated impinge on the surface on cooling, and is responsible for the increased coverage observed (Fig. 1). These observations are reasonably consistent with previous reports correlating surface coverage and temperature, where an annealing and cooling cycle results in a saturated lipid film.[40]

E. Diffusion measurements

In order to evaluate the mobility and homogeneity of the membranes on a microscopic-length scale, continuous
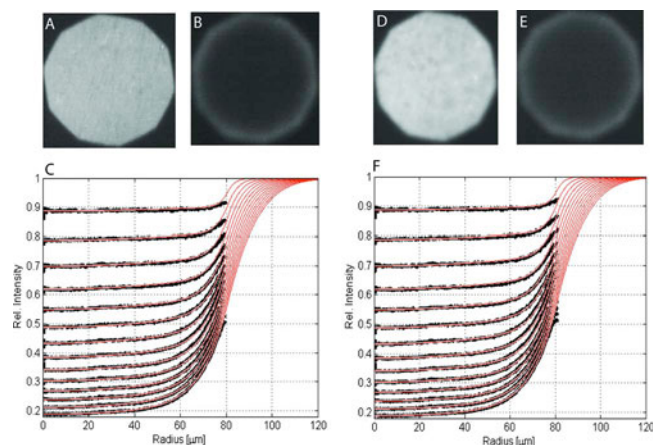
FIG. 7. (Color online) Continuous bleaching showing lipid diffusion in Oregon green-labeled DMPC SLBs prepared using the solvent-exchange method [(a) and (b)] and vesicle fusion [(d) and (e)]. Average background-corrected intensity profiles from the edge to the center of a circular selection made from the decagonal sample were used in obtaining the bleaching rate, which was subsequently used in calculating the diffusion constant based on fitting these profiles by the equations specified in the methods section [(c) and (f)]. The diffusion constant obtained for both SLBs was 2.6 ± 0.3 $\mu m^2/s$. Micrographs (a) and (c) were taken at $t=0$, and micrographs (b) and (e) were taken at $t=1$ min. For the experiments, illuminated regions with an approximate diameter of 180 μm were used. Continuous bleaching experiments were also performed for longer-chain SOPC membranes, and were found to have a diffusion constant of 2.3 ± 0.4 $\mu m^2/s$ (data not shown).

bleaching experiments were used. We directly compared supported lipid bilayers prepared using the solvent exchange method to those prepared by vesicle fusion. Lipid bilayer deposition onto a glass surface by solvent exchange was achieved using a flow-through sample chamber filled with lipid in an 8:2 water:isopropanol mixture. The water content was subsequently increased by the slow titration of the lipid solution. These were compared to membranes generated through small unilamellar vesicle fusion according to standard protocols.[12,37,41,42] A visual evaluation of the membranes produced by solvent exchange and vesicle fusion shows that both are homogeneous [Figs. 7(a) and 7(d)]. The samples were subsequently bleached continuously to evaluate its fluidity. In continuous bleaching, illumination is concentrated on a circular spot of the membrane using a field aperture. If a membrane is fluid, the fluorescence signal at the center of the illuminated area decays exponentially over time, while a fluorescence rim forms at its periphery. The latter results from the continuous diffusion of unbleached, fluorescently labeled lipids from the surrounding nonilluminated area. Both samples exhibit these characteristics of fluid membranes [Figs. 7(b) and 7(e)]. Evaluation of the diffusion data of the monolayer in contact with the surface indicate that membranes formed through solvent exchange have diffusion constants of 2.6 ± 0.3 μm^2 s^{-1} comparable with those obtained by vesicle fusion protocol, which is found to be also 2.6 μm^2 s^{-1} within experimental accuracy (Fig. 7) (for details, please refer to the experimental section). The measured diffusion constant consistent with the value 2.0 ± 0.4 μm^2 s^{-1} obtained for a DMPC bilayer prepared by

the vesicle fusion technique.[41,42] For comparison, the reader is reminded that in a free lipid bilayer, the diffusion constant of DMPC lies at about 0.5–5 μm^2 s^{-1} at room temperature.[41] For this protocol, the washing steps to remove excess alcohol are important; otherwise, the presence of a significant amount of residual alcohol would tend to increase membrane fluidity as a result of its H-bonding with the hydrocarbon chains, which then leads to a decrease its conformation order.[43]

F. Conclusion

We have investigated the phase behavior of the tenary system comprised of lipid, isopropanol, and water as a function of water content, temperature, and lipid head group. From SAXS and ATR-FTIR measurements, the bulk phase behavior was found to correlate with the amount of surface coverage. With increasing water content, the system undergoes phase transitions through the bulk phases: inverted micellar-monomeric-micellar-vesicles. At the same time, the coverage of lipid on the silicon oxide surface of the ATR crystal increases monotonically, reaching the saturating level of a single lipid bilayer coating. There are remarkable differences between the behavior of DMTAP and DMPC, with DMTAP exhibiting a steep increase in coverage as opposed to DMPC, which shows gradual deposition with increasing water content. This indicates that DMPC has a higher affinity for the solid than the cationic DMTAP, despite the fact that the solid is negatively charged. We also argue that within the transition regime from micelles to vesicles, the formation of solid supported bilayer is energetically favored over vesicle formation in the bulk phase due to the fact that surface interactions enhance the relative concentration of lipids at the surface. From this, we can define a protocol for depositing a lipid bilayer, which involves the incubation of a surface with a tenary mixture below this critical micelle-to-vesicle transition and gradually increasing the water content. A theoretical basis for this can be taken from the thermodynamics of alcohols interacting with lipid membranes.[44,45] We assume that the lipid aggregates at the solid surface, either monomers or micelles, are in thermodynamic equilibrium with the bulk phase. As the solvent is varied toward a pure water phase, the critical micelle concentration for the lipid is lowered and the lipids bound on the surface close to form a bilayer. This is in contrast to the vesicle fusion method, where lipid deposition takes place via vesicle rupture, an event that is associated with a high energy barrier. Additionally, lipids are required to spread and anneal at the surfaces after vesicle fusion. Hence, in special cases, where vesicle fusion or spreading is limited, as the case is for hydrophobic or nanostructured surfaces, the solvent exchange method might be advantageous for the formation of a supported bilayer.[24] Compared to vesicle fusion, this method has a clear shortcoming in that incorporation of proteins and precise control over composition are not guaranteed, and would require further investigation. For cases where a one-component lipid coating is required, however, the solvent-exchange protocol has advantages in terms of its applicability to complex structures, such as nanocontainers,

microfluidic devices with extended networks, or solid particles. In particular, the surface functionalization of microfluidic channels with solid supported bilayers, which aims to reduce protein-wall interactions, is an example where the solvent exchange technique can be applied.[46] For this kind of technology-driven applications, the ease of preparation is of primary importance, and the method presented here might have most impact.

ACKNOWLEDGMENTS

[1] E. Sackmann, Science **271**, 43 (1996).

[2] M. Tanaka and E. Sackmann, Nature (London) **437**, 656 (2005).

[3] J. Spinke, J. Yang, H. Wolf, H. Ringsdorf, and W. Knoll, Biophys. J. **63**, 1667 (1992).

[4] Y. Chan and S. Boxer, Curr. Opin. Chem. Biol. **11**, 581 (2007).

[5] B. Sanii and A. Parikh, Annu. Rev. Phys. Chem. **59**, 411 (2008).

[6] J. Groves, N. Ulman, and S. Boxer, Science **275**, 651 (1997).

[7] C. Steinem, A. Janshoff, W. P. Ulrich, M. Sieber, and H.-J. Galla, Biochim. Biophys. Acta **1279**, 169 (1996).

[8] S. Lenhert, P. Sun, Y. Wang, and H. Fuchs, Small **3**, 71 (2007).

[9] S. Gritsch, P. Nollert, F. Jähnig, and E. Sackmann, Langmuir **14**, 3118 (1998).

[10] D. Olson, J. Johnson, P. Patel, E. S. G. Shaqfeh, S. G. Boxer, and G. G. Fuller, Langmuir **17**, 7396 (2001).

[11] V. Kahl, M. Hennig, B. Maier, and J. Rädler, Electrophoresis **30**, 1276 (2009).

[12] M. Hochrein, J. Leierseder, L. Golubovic, and J. Rädler, Phys. Rev. Lett. **96**, 038103 (2006).

[13] J. Groves, Curr. Opin. Chem. Biol. **10**, 544 (2006).

[14] I. Czolkos, Y. Erkan, P. Dommersnes, A. Jesorka, and O. Orwar, Nano Lett. **7**, 1980 (2007).

[15] L. Tamm and H. McConnell, Biophys. J. **47**, 105 (1985).

[16] H. McConnell, T. Watts, R. Weis, and A. Brian, Biochim. Biophys. Acta **864**, 95 (1986).

[17] E. Kalb, S. Frey, and L. Tamm, Biochim. Biophys. Acta **1103**, 307 (1992).

[18] J. Nissen, S. Gritsch, G. Wiegand, and J. Rädler, Eur. Phys. J. B **10**, 335 (1999).

[19] J. Raedler, H. Strey, and E. Sackmann, Langmuir **11**, 4539 (1995).

[20] U. Mennicke and T. Salditt, Langmuir **18**, 8172 (2002).

[21] C. J. Brinker, Y. Lu, A. Sellinger, and H. Fan, Adv. Mater. (Weinheim, Ger.) **11**, 579 (1999).

[22] E. Sackmann and M. Tanaka, Trends Biotechnol. **18**, 58 (2000).

[23] F. Giess, M. G. Friedrich, J. Heberle, R. L. Naumann, and W. Knoll, Biophys. J. **87**, 3213 (2004).

[24] M. Hochrein, C. Reich, B. Krause, J. Radler, and B. Nickel, Langmuir **22**, 538 (2006).

[25] T. Bayerl and M. Bloom, Biophys. J. **58**, 357 (1990).

[26] F. Tiberg, I. Harwigsson, and M. Malmsten, Eur. Biophys. J. **29**, 196 (2000).

[27] F. Szoka and D. Papahadjopoulos, Proc. Natl. Acad. Sci. U.S.A. **75**, 4194 (1978).

[28] J. Strassburger and I. Smith, Appl. Spectrosc. **33**, 283 (1979).

[29] E. Goormaghtigh and J. Ruysschaert, Spectrochim. Acta, Part A **50**, 2137 (1994).

[30] J. Kalus and M. C. Gerstenberg, Phys. Scr. **T49B**, 629 (1993).

[31] N. P. Franks and Y. K. Levine, Mol. Biol. Biochem. Biophys. **31**, 437 (1981).

[32] G. Pabst, M. Rappolt, H. Amenitsch, and P. Laggner, Phys. Rev. E **62**, 4000 (2000).

[33] O. Glatter and O. Kratky, *Small Angle X-Ray Scattering* (Academic, London, 1982).

[34] J. S. Higgins and H. C. Benoît, *Polymers and Neutron Scattering* (Oxford Science, New York, 1994).

[35] C. Dietrich, R. Merkel, and R. Tampé, Biophys. J. **72**, 1701 (1997).

[36] M. Horton, C. Reich, A. Gast, J. Rädler, and B. Nickel, Langmuir **23**, 6263 (2007).

[37] R. Zantl, *Diplomarbeit* (Technische Universität, München, 1997).

[38] F. Ricoul, M. Dubois, T. Zemb, and D. Plusquellec, Eur. Phys. J. B **4**, 333 (1998).

[39] M. D'Angelo, G. Onori, and A. Santucci, J. Chem. Phys. **100**, 3107 (1994).

[40] E. Reimhult, M. Zch, F. Hk, and B. Kasemo, Langmuir **22**, 3313 (2006).

[41] C. K. Yee, M. L. Amweg, and A. N. Parikh, J. Am. Chem. Soc. **126**, 13962 (2004).

[42] M. P. Goertz, B. L. Stottrup, J. E. Houston, and X. Y. Zhu, J. Phys. Chem. B **113**, 9335 (2009).

[43] M. Patra, E. Salonen, E. Terama, I. Vattulainen, R. Faller, B. W. Lee, J. Holopainen, and M. Karttunen, Biophys. J. **90**, 1121 (2006).

[44] P. Westh and C. Trandum, Biochim. Biophys. Acta **1421**, 261 (1999).

[45] J. Schellman, Biophys. Chem. **37**, 121 (1990).

[46] R. Galneder, V. Kahl, A. Arbuzova, M. Rebecchi, J. O. Rädler, and S. McLaughlin, Biophys. J. **80**, 2298 (2001).